ISSN 1392–1320 MATERIALS SCIENCE (MEDŽIAGOTYRA). Vol. 29, No. 4. 2023

Mechanical and Microstructural Characteristics of Rotary Friction Welded SS316L and Pure Copper with Added MWCNT Nano Additives

Martin Charles MARK [1*], Satish Kumar SHANMUGAM [2], Ramadoss RAJENDRAN [3]

[1] *Department of Mechanical Engineering, Loyola-ICAM College of Engineering and Technology, Nungambakkam, Chennai, TamilNadu, India, 600034*
[2] *Department of Mechanical Engineering, Velammal Engineering College, Surapet, Chennai, India, 600066*
[3] *Department of Mechanical Engineering, Easwari Engineering College, Ramapuram, Chennai, India, 600089*

https://doi.org/10.5755/j02.ms.33038

Received 24 February 2023; accepted 19 April 2023

This study explores the novel design of geometric rubbing profiles on rotary friction welding for enhanced mechanical clamping in joining dissimilar alloys such as copper and stainless steel 316L. The clamping behavior of rubbing profiles could hold the yielding of the weld joint to a maximum level. An innovative approach to effective mixing of the weldment zone could be achieved through the definition of rubbing profiles. The effective dispersion of dissimilar metallic phases could be governed by the geometrical profile in achieving the intermetallic SS-Cu phase. Variations were made in welding parameters like tool rotational speed, upset pressure, upset time, friction pressure, and friction time to find the appropriate process for the four different rubbing profiles, namely helical fluke, plus, cylindrical, and flat to achieve a reduction in micro and macro-structural defects with strong weldnugget. Results show that helical fluke rubbing profiles were seen to have explicit values like ultimate tensile strength of 217 MPa (upset pressure), elongation of 9.8 % (upset pressure), and average hardness of 125 HV (friction pressure) at the weld nugget. Microstructural characteristics prove that the formation of IMCs through grain size reduction such as cementite increases the Vickers hardness ofthe weldment.
Keywords: rubbing, profiles, rotary, friction, welding, MWCNT, geometric, weldment.

1. INTRODUCTION

Joining issimilar metals as an engineering structure poses extensive behavior. It not only enriches hybrid nature but also exhibits corrosion resistance, ductility, high thermal conductivity, etc. [1]. The formation of a composite structure with SS316L and copper will reduce cost considering the other precious metals of the same nature. With the great difference in their thermomechanical properties, joining dissimilar materials by traditional methods is very difficult. Existing methods of joining dissimilar metals are laser welding,ultrasonic welding, forge welding, brazing, electron beam welding, plasma welding, etc. These methods arenot cost-effective or time effective. Due to the working nature at high temperatures, these are likely to cause oxidation, cavities, and cracking problem.

The compo-casting method is a well-known method to create metal-based matrix composites, but the lack of desirable mechanical properties due to weak bonding strength and uneven distribution of reinforced subdivisions makes it unsuitable for dissimilar joining. [2 – 4].

The accumulative press bonding (WAPB) and accumulative roll bonding (WARB) processes are solid-phase cladding methods of bonding dissimilar metals. The poor bond strength is one of the major drawbacks of the processes [5, 6].

Works were carried out on the comparison of stirring and press/roll bonding methods. It has been concluded that the stirring method creates efficient severe plastic deformation in obtaining the uniform grain boundary cracking in comparison to the press bonding technique [7, 8].

To surpass these issues a novel welding/stirring technique through RFW/RFS is possible to give a robust weldment [9]. Viscoplastic deformation, softening, and plasticization of dissimilar metals make a uniform dispersion of phase molecules. Also, dissimilar joints are potentially beneficial for high metallurgical reactivity and affinity between SS316L and copper. There again is the formation of Intermetallic Compounds (IMC) which in turn results in low weld strength. A defect-free weld between SS316L and copper must beevolved. To overcome all these hurdles an optimum methodology must be adopted to produce an effective ring in the nugget zone. This could be attained through the placement of the workpiece on the advancing side or retreating side, with parameters (rotation rate and welding speed) [10]. These key factors have been investigated since then to affect the type of IMCs produced as well as the distribution of IMC in the welds. It is necessary to place the harder SS316L on the advancing side [11]. For each feed step, it is easier to soften the harder material. Different behavior is likely to ease the flow of softer material namely copper when it is placed on the retreating side so that it can be transported to the advancing side. This results in good mixing of materials [12]. Brittle intermetallic compounds and high thermal conductivity are the two problems normally encountered in this welding. Various ferrous and non-ferrous alloys having circular or non-circular cross sections and having different thermal and mechanical properties can be easily joined by friction

* Corresponding author. Tel.: +917502842211.
E-mail: *martincharles.m@licet.ac.in* (M.C. Martin)

welding. Friction time, friction pressure, forging time, forging pressure, and rotation speed are the principal welding variables in friction welding. Shanjeevi et al. (2014) investigated the mechanical, thermal, and metallurgical properties of friction-welded steel copper bars [13]. Kumar et al. (2015) examined the irradiation resistance of copper and titanium joints fabricated by friction welding methods [14]. Lee et al. (2022) investigated the effect of microstructure variation on Cu/C 45 carbon steel friction welding [15]. Joining dissimilar metals is best done by friction welding, due to the advantages of friction welding. Saving in the material can be realized while joining large-diameter rotor bodies on other rotating members [16]. The same is the case with the joining of the components of valve systems.

Many of the electrical parts today are being manufactured by combining metal forming and metal joining routes. Actuator sensors, transducers, and safety devices find wide applications in industries, to mention a few examples. Aluminum can be welded to copper for the mass production of cable lugs used in transformers. The effect of strain and the rubbing profile to ensure good joints in such cases with sound weld properties is the main objective. Some of the profiles usually come across are round profiles, angular profiles, stepped profiles, and flat profiles. For the angular profile, the samples for the test are machined to an angle of 45° and 60°. In the stepped profile protrusions were made on the pre-strained aluminum side and the corresponding recess will be made on the copper side. Protrusions of length depend on the diameter of the bar. The usual parameters of friction pressure, upset pressure, burn off length are controlled during welding. The welded pieces were subjected to mechanical and microstructure characterization for optimizing the process parameters. The friction welded samples were longitudinal to analyze the metal flow during welding. Other rubber profiles than flat and stepped profiles failed while bifurcating the friction-welded specimens. This is due to poor metallurgical bonds. Visual observation of samples with flat profiles showed a wavy interface indicating a good joint observation on the sectioned samples of stepped profile revealed that titanium had penetrated copper by deforming it. The straight protruded part of the titanium sample bulged into a dovetail shape as the process parameters were increased [17]. The same was not observed in the case of other geometry. As protrusion length was increased the formation of a dovetailed shape was not much pronounced. Upon testing the samples for mechanical properties, it was found that round profile and angular rubbing profiles failed while machining the samples. This was due to the poor bonding of the weld. This was because lower friction and upset pressure resulted in less inter-atomic diffusion of the materials, thus forming a poor joint. The fractured surface of copper revealed a pale grey aluminum layer which may contain a substantial amount of intermetallic compounds as far as the flat rubbing profile was concerned [18].

The metallurgical bond along with the mechanical interlock resulted in good weld strength for a stepped profile with a 5 mm protrusion length. Friction welding with a stepped profile thus resulted in a metallurgical bond along with a mechanical interlock. Thus, the initial geometry of samples had a large influence in deciding the weld strength. The use of nano additives as MMC for weldment creates enhanced strength and reinforcement. The nanoparticles in the weldment zone produce effective reinforcement based on microstructure and mechanical properties. The uses of SiC particles as reinforcement during the friction welding process improvise the microhardness of weldment. It has been remarkably noted that the tensile strength, fatigue life, and toughness of joints have been improved. This factor creates a growth in grain boundary hindered because the pinning effect of SiC led to enhanced tensile properties. The other use of B_4C and Al_2O_3 also provides robust reinforcement capabilities. It has been also stated that the size of the reinforcement particle is very crucial in deciding the properties of MMC their particle size affects the joint properties most significantly. With the increase in particle size, the tensile strength and the hardness decreases. The impact of process parameters on rotational speed creates a higher tensile strength, elongation, and ductile mode fracture the placement of a higher amount of nanoparticles. Also, the use of metal oxides such as TiO_2 and TiC as reinforcement material enhances the tensile properties. The use of carbonaceous materials namely CNT and graphene have monitored major attention as a prospective reinforcing nanomaterial in friction welding, due to their exceptional mechanical, chemical, thermal, and tribological properties [19]. By considering the significance of rotary friction welding with various types of nanomaterial reinforcement and their correlations, it is many joining properties and tactics to in situ deposition are yet to be discovered and studied attentively.

Research in the domain of carbon was revamped by carbon nanotubes (CNTs) and graphene which have been trenched as wonder materials. The use of graphene and CNTs reinforcing abilities has produced benchmarking concepts across the globe. Thus, CNTs and graphene emerged as ideal reinforcement for composite structures due to their intrinsic characteristics and exceptional physical, mechanical, electrical, and thermal properties. Owing to these excellent properties, a study was conducted in the field of rotary friction welding to make composites. Carbonaceous nanomaterials accommodate its adequate interfacial bonding with the matrix of the composite. During RFW in the NZ, CNT tubular morphology was retained even with severe deformation. However, a reduction in the length of CNT was reported from about 150 nm to about 80 nm. The size of the grain in the nugget zone is coarsened to about 400 nm. It is due to the combination of severe deformation and heat input as earlier researchers reported that composite CNT/Al grain size would remain stable when subjected to annealing at 723 K. Researchers reported dissimilar thermoplastic friction stir welding between high-density polyethylene (HDPE) and Acrylonitrile Butadiene Styrene (ABS) reinforcing with multi-walled carbon nanotubes (MWCNTs). A groove was fabricated with different widths such as 0.2 mm, 0.3 mm, and 0.4 mm, on the ABS plate, to accommodate different volume fractions of MWCNTs reinforcement. After filling MWCNTs into the groove of the ABS plate, the HDPE plate was placed at the top surface of the ABS plate. Another application of carbon-based nanomaterial-reinforced FSW besides enhancing joining strength is to make Carbon nanotubes reinforced Al composite foam. The authors fabricated a foamable

precursor, by mixing titanium hydride (TiH_2) as blowing agent powder and carbon nanotubes (CNTs) as reinforcement into 1.5 mm thick AA1080 aluminum sheets the by using FSW route. Subsequently, the closed-cell Carbon nanotubes and Aluminium composite foams are obtained by placing of precursor in a furnace for foaming. For this, three aluminum plates were stacked and clamped for the FSW process. Before stacking, the TiH_2 and CNTs were distributed homogeneously into each AA1080 plate. An overlapping FSW with multi passes has been performed to mix segregated TiH_2 and CNTs uniformly. Thus, we can see that for improving joint strength of similar as well dissimilar material which has ineffective joint properties, ceramic and carbonaceous nanomaterials reinforcement work effectively. The effectiveness of nanomaterials reinforcement in FSW can be understood through microstructural examinations as well as mechanical, tribological, chemical, and electrical analysis. The novel approach with the implementation of geometric rubbing profiles in the workpiece could improve the tensile properties based on the breakdown of the Orawan strengthening effect. This could reduce the precipitation-hardening effect on the weld bead and thereby reducing the formation of intergranular cracks. The clamping behavior of rubbing profiles could hold the yielding of the weld joint to a maximum level. Excellent fusion formations would be produced at the sidewalls of the groove and the interlayers without any observed defects, such as holes, inclusions, or macro-cracks. It could be observed that phases were homogeneously distributed in the weldment. An efficient mixing mechanism could be drawn for the proper dispersion and mixing of the phase materials to ensure the mechanical strength and fine-grain dispersion of microparticles to enrich the bondage of the weld zone.

2. EXPERIMENTAL METHODS

The welding materials as stainless steel and pure copper have been fabricated with the considerations of pin profiles like a fluke, cylindrical pin, and pattern. Three different profiles were used as flat, plus and fluke as shown in Fig. 1 were used for the rotary friction welding. The mechanism of the proposed method is shown in Fig. 2. This discusses the influence of pinned rubbing profiles of various shapes like plus and fluke patterns which improve the stirring efficiency of the rubbing profile. Effective stirring action at the weld surface was prompted with higher frictional force. Mechanical clamping to increase the bonding of dissimilar metals. Male and female sockets can create plunged bondage to enhance the Mechanical strength at the weld joint. Flat, cylindrical, plus, and fluke shape sockets are made on the surface edges. Fluke shape is effective due to more stirring of metals at the metal surfaces.

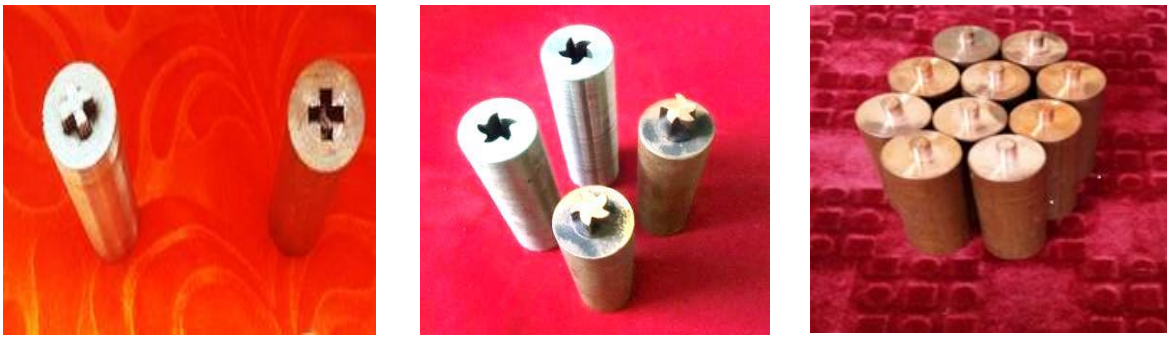

a b c

Fig. 1. Photographic view of the geometric Rubbing profiles: a – plus profile; b – fluke profile; c – cylindrical pin profile

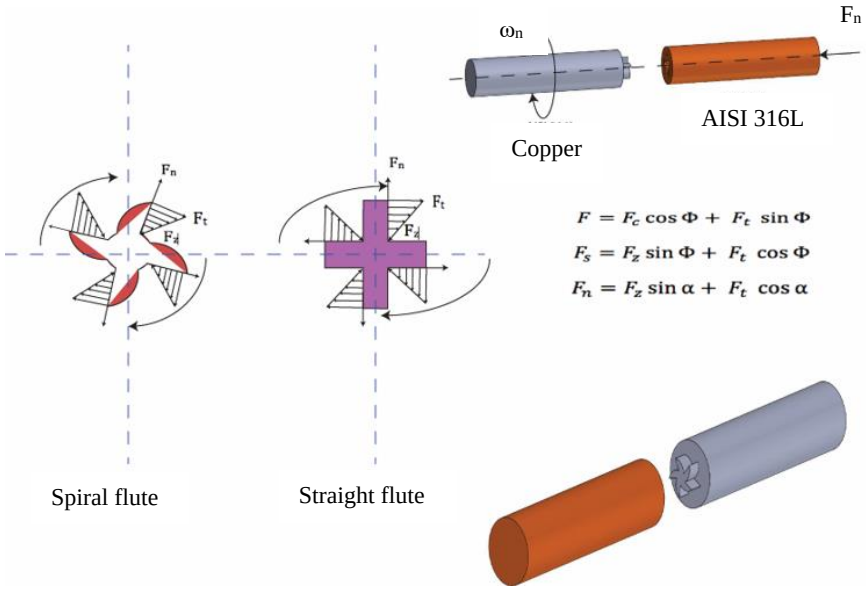

Fig. 2. Mechanism of profiled sockets in rotary friction welding

The fluke shape is made of harder metal (copper) and hollow sockets are made of soft metals (stainless steel). Atomic structure and molecular pattern ultra-fine grain size is formed at the HAZ (heat-affected zone). The formation of oxides and intermetallic compounds after welding reduces the weld strength at the weld interface. The chemical composition and mechanical properties of the stainless steel and copper are shown in Table 1 and Table 2.

The male socket profile is considered to be a cylindrical, fluke, plus a pattern with a height considered to be 8 mm. In the female socket, the depth is considered to be 8 mm. Stainless steel SS316L and Pure copper rods with 20 mm diameter and 80 mm length are joined through a Rotary Friction welding process. The profile rubbing edges are to be joined with the process parameters. The welds were processed using the parameters shown in Table 3.

Table 3. Process parameters and material dimension

Welding parameters	Range	Unit
Friction pressure	55 – 80	MPa
Friction time	10 – 20	sec
Rotational speed	1000 – 1500	rpm
Upset pressure	100 – 250	MPa
Upset time	5 – 10	sec
Material diameter	20	mm
Material length	80	mm

Initially, the experiments were conducted according to the design of experiments formulated through central composite design. The framed experiments were initiated through the addition of MWCNT particles on the nugget zone to reinforce the strength of the weldments.

To progress this work four different profiles are designed (flat, cylindrical, plus, helical flute) over the sides of the weld nugget zone for the filling of MWCNT particles. The process is patterned according to the patterns of the slotted male and female sockets. The MWCNT particles were purchased from Shilpent, Maharastra, India with a particle diameter of 10 nm and length of 10 µm. The impurities were washed with methanol under a centrifugation process under 2000 rpm for 15 min. The moisturized MWCNT slag was air dried in a hot air oven under 120° Celsius for 2 hours.

The dried MWCNT particles were compacted in the female socket of the SS316L rod as shown in Fig. 3.

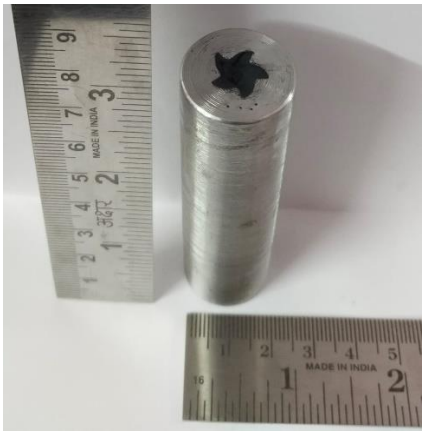

Fig. 3. Infill of MWCNT particles in the female socket of SS316L

The main objective of the proposed work is to improve the mechanical strength of the weldments through a clamping mechanism. Hence the work is tabulated as flat, cylindrical, plus, and fluke patterns. The output responses of mechanical characterization, microstructural characteristics, material flowability characteristics were evaluated for the weldments. The photographic views of the welded samples are shown in Fig. 4.

Table 1. Chemical properties of Base metals

Material	Cr	Ni	Mo	C	Mn	P	Su	Si	Fe	N
AISI 316L steel	17	12	2.5	0.030	2.0	0.045	0.03	0.75	Balance	0.1

Table 2. Mechanical properties of base metals

S. No	Material	Tensile strength, MPa	Elongation, %	Izod Impact, J	Vickers hardness, HV
1	SS316L	280	15	18	105
2	Copper	226	25	26	73

Fig. 4. Photograph of the welded samples

The samples of the tensile test were prepared with the following steps for all the weldments. The dogbone specimens were prepared for the 8 specimens based on their welding methods to ensure the specimens are free from debris. Check for any nicks, dents, scratches, or other deformations that will change the shape of the specimen. The samples were cleaned using acetone to etch the surface. The samples were cut according to the specific dimensions as shown in the figure. Using wire-cut EDM the profile is machined according to the ASTM standards. Tensile specimens were maintained with a gauge length of 50 mm and width of 12.5 mm. The microstructural analysis through an optical microscope (Moticam 1000, China) having a 25× lens zooming capacity, determines the effective dispersion of MWCNT particles in various rubbing profiles. It is aided through an image processing approach through MATLAB software. The specimens were cut by a sawing process with cooling water attached for maintaining a low temperature on the cutting zone and to avoid grain refinement. The samples were then etched using Potassium Dichromate & Keller soln. The sectioned specimens were mounted by thermosetting resin for effective edge retention. Mounted specimens were ground using an automated device, which consisted of a SiC abrasive sheet. The specimens were ground using a series of abrasive sheets of grit sizes ranging from 60 to 50 microns. The images are acquired at the weld nugget zone where the MWCNT particles are dispersed.

These images are preprocessed using a contrast thresholding procedure to differentiate the boundaries of MWCNT, Stainless steel, and copper layers. The contrast thresholding is evaluated through the pixel intensity value of 0 – 255. The image is segmented through the region of interest segmentation as shown in Figure. The region of interest holds the boundary of the MWCNT particles to be traced off using a polyline masking method. This method is used to trace and mask the MWCNT particles in the image plane. The segmented MWCNT particles are located in the pixel region with its array location. This array location is used to convert the image in binary conversion for extracting the region of MWCNT particles and Stainless steel/copper zones.

The binary image conversion is processed through Otsu's thresholding of gray-level image segmentation for the conversion of grayscale image to binary image with zeros and ones to easily segregate the boundary layer of the MWCNT and Stainless steel or copper particles in the image plane as shown in Fig. 5. The array of rows and columns was binarized according to the pixel data. The pixel data is converted to distance using the Euclidean distance measurement principle, which converts the pixel into the respective distance with metric calibration. This is used to evaluate the distance of the MWCNT boundaries. In our case, there is a need to evaluate the area of the boundaries, which defines the differential value of the metallic and MWCNT phases. The dispersion ratio is calculated as the ratio of the area of the metal phase occupied in the image region to the MWCNT particles occupied in the image region. With the calculation of the dispersion ratio, we can evaluate the percentage of MWCNT dispersion on the weldment zone.

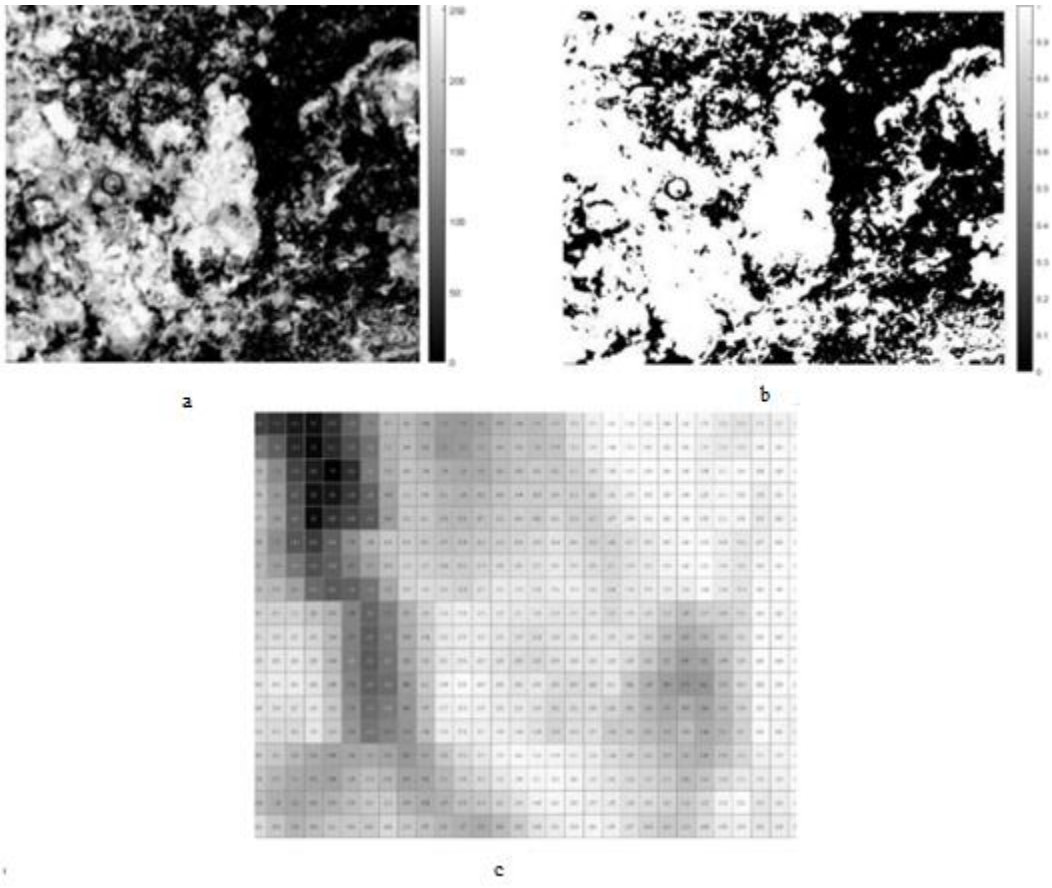

Fig. 5. a – contrast thresholding; b – image segmentation; c – pixel to distance conversion

Vickers hardness is used to identify the indentation of the load spread over the micro surface area when the diamond v-cross indenter is hinged on the weldment surface. The samples were subjected to a load of 1 to 100 kgf for 10 to 15 seconds. The resulting impression should have well-defined points of measurement. The two diagonals of the indentation left on the surface of the material after removal of the load is measured using a microscope and their average is calculated. Effective stirring action at the weld surface was prompted with higher frictional force.

3. RESULTS AND DISCUSSION

The ultimate tensile strength values are maximum for the helical profile compared to the other three, the values are optimal at a speed of 1100 rpm, and they gradually reduce to low values at 1500 rpm. The ultimate tensile strength for a helical rubbing profile is 210 MPa at 1100 rpm, at the same speed it is 205 MPa for the plus profile. For a cylindrical profile, the optimal value is 193 MPa. For a flat rubbing profile ultimate → tensile → strength → that 1100 rpm happens to be 185 MPa, on the lower side at 1500 rpm the ultimate tensile strength for the helical profile is 193 MPa. For plus profile Ultimate tensile strength is 184 MPa at the same 1500 rpm for the cylindrical profile UTS is found to be 177 MPa and for the flat rubbing profile ultimate tensile strength happens to be 164 MPa, at the same rpm. When the comparison of the other three peak values with that of the helical profile in percentage is made, for plus profile the deviation with the helical profile is 2.3 % for cylindrical profile the deviation for peak value compared to the helical profile is 8.09 % for the flat profile the variation for peak value compared to helical profile is 16.6 %. At low speeds heat that is produced is quite low, due to insufficient heat the welding bond that is produced is poor. As speed increases there is sufficient heat flux that is generated. This gives good plasticity and good quality weld joint is produced thus the UTS increases gradually and reaches peak or optimal value. Beyond a certain speed due to high heat, IMCs are formed which will reduce the strength of the joint. Hence after the optimum point, the curve gradually sloped downward the graph of ultimate tensile strength shown in Fig. 6 , concerning upset pressure varies from the lower value to a peak value and gradually decreases to a low value. It can be seen that optimal values of ultimate tensile strength UTS are occurring at an upset pressure of 160 MPa, at that pressure the ultimate tensile strength UTS for helical profile is 217 MPa. At the same pressure for plus profile the Ultimate tensile strength UTS for the plus profile, cylindrical profile flat profile and is 200 MPa, 191 MPa, and 185 MPa respectively. The Low values of Ultimate tensile strength UTS at an upset pressure of 250 MPa are observed to be 205 MPa for the helical profile, 192 MPa for plus profile, 180 MPa for the cylindrical profile, and 176 MPa for the flat profile. On comparing the peak values of the helical profile with the other three profiles. For the plus profile, the variation in peak value compared to the helical profile is 3.2 %, for the cylindrical profile the variation in peak value compared to the helical profile is 11.9 %, for the flat profile the variation in peak value compared to helical profile is 14.7 %.

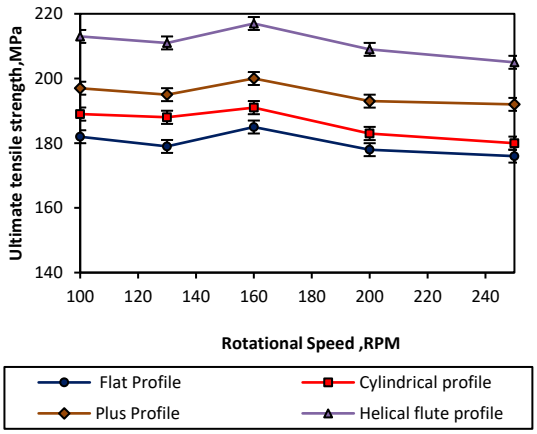

a

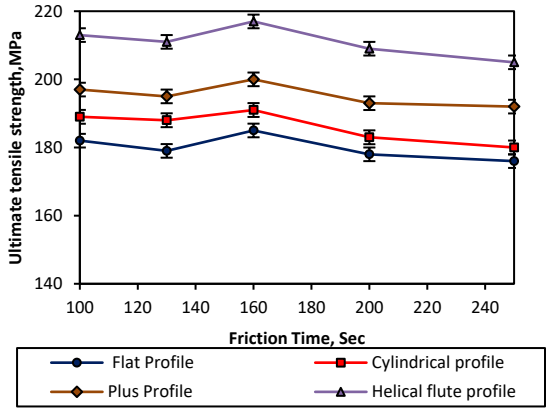

b

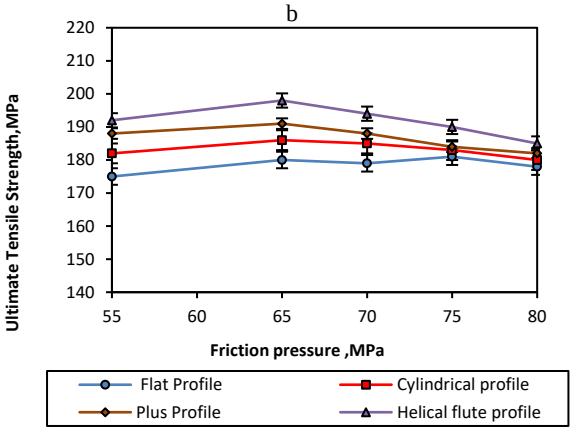

c

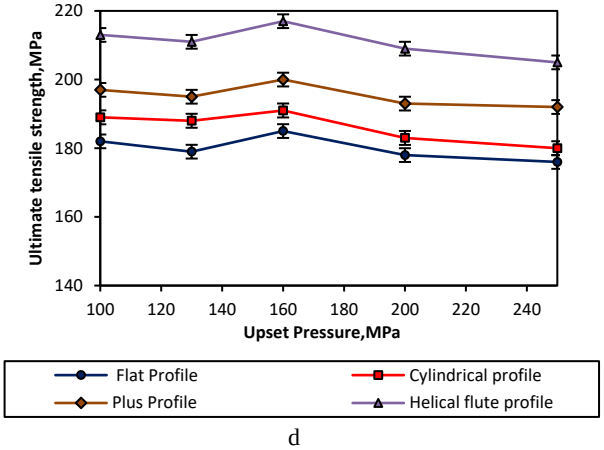

d

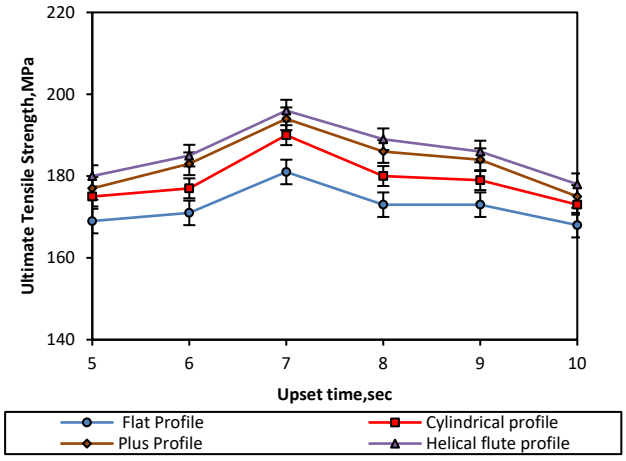

e

Fig. 6. Effect of various rubbing profiles for ultimate tensile strength vs. process parameters: a – ultimate tensile strength vs. upset pressure; b – ultimate tensile strength vs. friction time; c – ultimate tensile strength vs. friction pressure; d – ultimate tensile strength vs. upset pressure; e – ultimate tensile strength vs. upset time

The formation of the weld interface occurs at the highly deformed region, due to thermo- mechanical, and was obtained nearer to the weld interface. It also shows that partly deformed zone of stainless steel and copper dissimilar joints. On both sides of the partly deformed zone, the microstructure is fine-grained compared to the base metal microstructure. This is due to micro residual stresses caused by deformation. This increases the ultimate tensile strength value [21].

The ultimate tensile strength is maximum for the helical profile when compared to the other three profiles. The variation of ultimate tensile strength concerning friction pressure increases steadily with speed reaching a maximum and then reduces linearly afterward. Optimal values of ultimate tensile strength are obtained at a friction pressure of 65 MPa. The value of ultimate tensile strength at a friction pressure 65 MPa for helical profile is 198 MPa and at the same friction pressure. The ultimate tensile strength value for plus profile is 191 MPa for the cylindrical profile, it is 186 MPa, and for the flat profile, it is 180 MPa. Lower values of ultimate tensile strength are obtained at a friction pressure of 80 MPa. The value of Ultimate tensile strength at a friction pressure 80 MPa, for a helical profile is 185 MPa and at the same friction pressure. The ultimate tensile strength value for plus profile is 182 MPa for the cylindrical profile it is 180 MPa and for the flat profile it is 178 MPa comparing the other three peak values with that of the helical profile in percentage for plus profile, the cylindrical profile and the flat profile the variations for peak value compared to helical profile are 3.5 %, 6.06 %, and 7.06 %. respectively. The friction pressure characterizes the friction heating with the interfacial temperature field and its evolution, on which the corona bond initiates and spreads. This increases the viscoplastic state of the metal at the weld zone, which again leads to the formation of surface serrations due to the turbulence effect of the rubbing profiles in increasing the ultimate tensile strength value [22].

The graphs ultimate tensile strength concerning friction time increases up to a maximum value and then decreases thereafter gradually. The curve for the helical profile lies outermost and the curve for the flat profile lies innermost, the optimal values of ultimate tensile strength were observed at a friction time of 14 seconds. The ultimate tensile strength for the same friction time for the helical profile, plus profile, cylindrical profile, and flat profile obtained are 217 MPa, 200 MPa, 191 MPa, and 185 MPa respectively. The lowest values of ultimate tensile strength were obtained at an Upset time of 20 seconds. The ultimate tensile strength for the same friction time for the helical profile, plus profile, cylindrical profile, and flat profile obtained are 188 MPa, 182 MPa, 179 MPa, and 173 MPa respectively. On comparing the peak value of the helical profile with plus profile, cylindrical profile, and flat profile the deviation observed is 7.83 %, 11.9 %, and 14.7 % respectively. The reason for this is the parent particles were severely fragmented and new dynamic recrystallized grains evolved during the friction welding process. Consequently, the temperature effect and shear stress cause the conversion of the dislocation boundaries into new equiaxed fine grains.

A very fine, recrystallized microstructure accommodates high strains by the either continuous or discontinuous solid-state flow. The graphs of ultimate tensile strength UTS for upset time increase up to a maximum value and then decreases thereafter gradually. The curve for the helical profile lies outermost and the curve for the flat profile lies innermost. The optimal values of UTS were observed at a friction time of 7 sec. the ultimate tensile strength for the same friction time for the helical profile, plus profile, cylindrical profile, and flat profile obtained are 196 MPa, 194 MPa, 190 MPa, and 181 MPa respectively. The lowest values of ultimate tensile strength UTS obtained at an upset time of 10 sec. The ultimate tensile strength for the same friction time for the helical profile, plus profile, cylindrical profile, and flat profile obtained are 178 MPa, 175 MPa, 173 MPa, and 169 MPa respectively. On comparing the peak value of the helical profile with plus profile, cylindrical profile, and flat profile the deviation observed is 1.02 %, 3.06 %, and 7.6 % respectively.

The tensile strength of the welds with dissimilar joints possesses the lower weld strength when compared to their base metals strength. This is because of the improper stirring of the copper particles, which are harder to be mixed. The formation of the intermetallic components increases the influence of joint strength. This is because of the proper stirring of the base metals with the displacement of grain particles having different melting points and thermal conductivities.

The micro-Vickers hardness values are maximum for the helical profile compared to the other three. The values are optimal at a speed of 1100 rpm, they gradually get reduced to low values at 1500 rpm. The optimal value of micro-Vickers hardness at a speed of 1100 rpm for the helical rubbing profile is 137 HV, for plus profile the micro-Vickers hardness is 113 HV at the same speed. When it comes to the cylindrical profile the hardness is 105 HV. For a flat rubbing profile at the same speed the micro Vickers hardness is found to be 97 HV, on the lower side at a speed of 1500 rpm, the micro-Vickers hardness for a helical profile is 119 HV, For plus profile at the same speed the micro Vickers hardness is 101 HV, While for cylindrical profile the micro Vickers hardness at that speed is 95 HV

and for flat profile the hardness is 85 HV at the same speed. On comparing the peak value of the helical profile with the other three profiles as a percentage it is found that for plus profile the variation for peak value is 17.5 %, For the cylindrical profile the variation for peak value compared to the helical profile is 23.35 % and the deviation for flat profile for peak value compared to helical profile is 28.4 %. Different thermal diffusivity of materials and intermetallic layers existing at the interface causes the hardness variation, no significant variation is obtained in the grain size on the steel side, copper exhibits equalized grains and dispersion of Cu2O particles steel reaches the annealing temperature that reduces micro-Vickers hardness at higher speeds, copper exhibits micro-Vickers hardness due to high thermal conductivity and fast cooling behavior [23].

The micro-Vickers hardness values are maximum for the helical profile compared to the other three. The values are optimal at an upset pressure of 160 MPa and then they gradually reduce to low values at 250 MPa. Optimal values at an upset pressure 160 MPa. The micro-Vickers hardness for the helical profile is 121 HV at the same upset pressure for plus profile the micro Vickers hardness is 113 HV, for the cylindrical profile, the micro-Vickers hardness is 102 HV, and flat profile the micro-Vickers hardness is 95 HV, for low hardness values at an upset pressure of 250 MPa obtained will be 114 HV, 103 HV, 94 HV and 88 HV for helical profile, plus profile, cylindrical profile, and flat profile respectively. The deviation of peak values between the helical profile and the profile is 12.19 %, between the helical profile and cylindrical profile is 17 %, and between the helical profile and flat profile is 20.3 %.

The small properties disparity in both the materials resist deformation which positively increases friction at the cross section area leads to proper origination of heat effected zone which is suitable for good welding and it shows less effective results in the case of SS 316L and copper due to large parent properties disparity which leads to improper deformation due to less heat generation during welding. This increases the micro-Vickers hardness value.

The micro-Vickers hardness is maximum for the helical profile when compared to the other three profiles the variation of micro-Vickers hardness to Friction pressure increases steadily with speed reaches a maximum and then reduces linearly afterwards. The optimal value of micro-Vickers hardness at a friction pressure of 65 MPa for the helical profile is 125 HV, for plus profile the micro-Vickers hardness is 114 HV for the same friction pressure. For the cylindrical profile it is 105 HV and for the flat profile the micro it is 92 HV. Lower values of micro-Vickers hardness were observed at a friction pressure of 55 MPa, the micro-Vickers hardness values for helical profile, plus profile, cylindrical profile flat profile is 117 HV, 104 HV, 93 HV and 84 HV respectively. On comparing the other three peak values with that of the helical profile in percentage. For the plus profile, the deviation compared to the helical profile is 8.8 %, For the cylindrical profile the deviation compared to the helical profile is 16 %. For the flat profile, the deviation compared to the helical profile is 26.4 %. The proper intermixing of metallic alloys takes place. Instead increases the temperature at the thermo-mechanical affected zone with a larger amount of displacement of base alloys forming intermetallic components. The existence of brittle IMCs in the stir zone increases the hardness and leads to the formation of fragmental cracks. This reduces the micro-Vickers hardness value. The graphs shown in Fig. 7, of micro-Vickers hardness to friction time vary linearly, increasing gradually from lower to higher values.

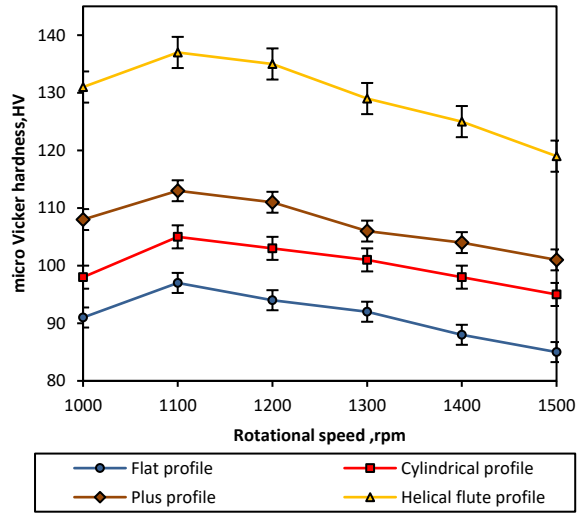

a

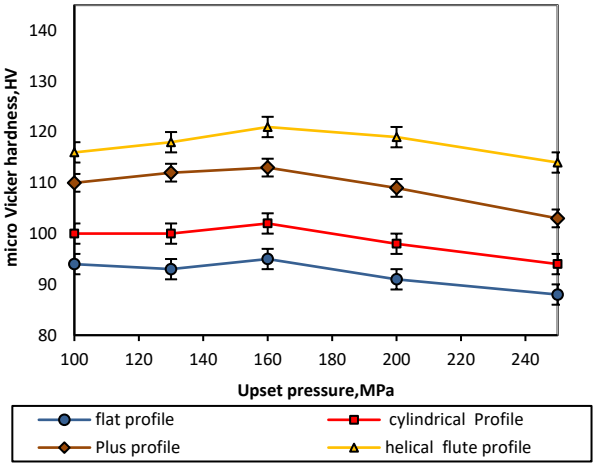

b

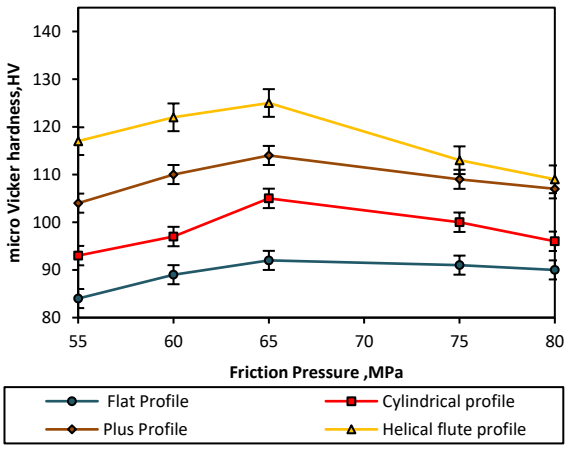

c

(Fig. 7 continued on the next page)

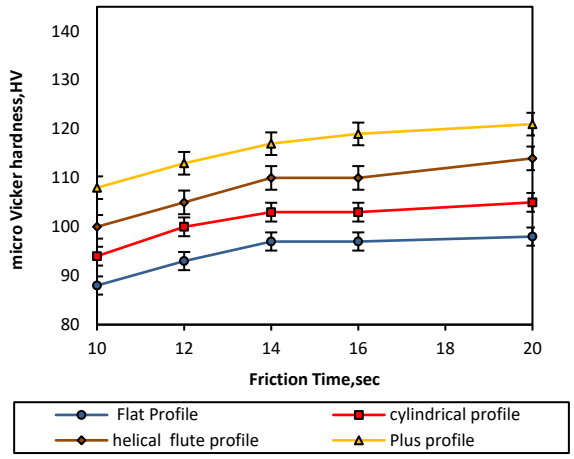

d

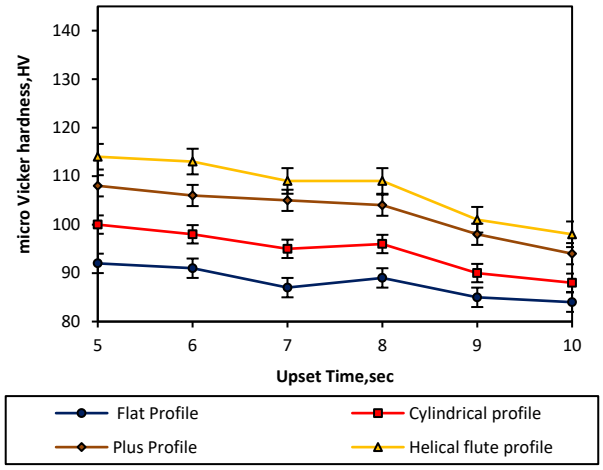

e

Fig. 7. Effect of various rubbing profiles for micro-Vickers hardness vs. process parameters: a – ultimate tensile strength vs. rotational speed; b – ultimate tensile strength vs. upset pressure; c – ultimate tensile strength vs. friction pressure; d – ultimate tensile strength vs. friction time; e – ultimate tensile strength vs. upset time

The lowest values of micro-Vickers hardness were measured at a friction time of 10-sec micro-Vickers hardness of helical, plus, cylindrical, and flat profile was measured at the same friction time is 108 HV, 100 HV, 94 HV, and 88 HV respectively. On comparing the peak values on comparing the other three peak values with that of the helical profile in percentage for plus profile the deviation compared to the helical profile is 5.78 %, forthe cylindrical profile the deviation compared to the helical profile is 13.2 %, for flat profile the deviation compared to helical profile is 19 %. At higher friction time there will be a difference in the cooling speed between the rotating and fixed sides. Furthermore, due to the limited heat capacity of the material on reduced cross-sectional areas, the cooling rate is also limited. Thus, the friction welding time for small-diameter rods will be different from that of large-diameter rods. The graphs of micro-Vickers hardness for upset time vary, decreasing gradually from higherto lower values. The curve for the helical profile lies outermostand the curve for the flat profile lies the innermost, optimal value of microhardness at an upset time of 5 sec for the helical rubbing profile is 114 HV, and for plus profile the hardness is 108 HV at the same upset time 5 sec when it comes to cylindrical profile the hardness is 100 HV. For the flat profile at the same speed, the hardness is found to be 92 HV. On the lower side at an upset time of 10 sec, the microhardness for the helical profile is 98 HV for the plus profile at the same upset time the hardness is 94 HV, while for the cylindrical profile, the microhardness is 88 HV. And for a flat profile, the hardness is 84 HVat the same upset time. On comparing the peak value of the helical profile with the other three profiles as a percentage it is found that for plus profile the variation for peak value is 5.26 %, and for the cylindrical profile the variation for peak value compared to the helical profile is 12.28 % and the deviation forflat profile for peak value compared to helical profile is 19.29 %. During processing, frictional heat and deformation strain is generated and result in continued plasticization of the interfacial region between the workpieces and displacement of plastically deformed material toward the weld edges to form a flash (upset metal). Once sufficient plasticization has occurred, a forging force is applied to produce a consolidated joint seam with the limited thermomechanically affected zone (TMAZ) and heat-affected zone (HAZ). If sufficient frictional heat has been producedduring the previous phase to soften the interface material, larger wear particles begin to be expelled from the interface,and axial shortening of the workpieces begins as a result ofthe expelled upset.

Some dendrites scars of SS316L have been observed in the TMAZ zone as shown in Fig. 8. The cleavage facet, where observed on the river flow pattern of the weldment. The extinction of copper and the formation of ultra-fine grains where occurred based on the boundary layer. Cracking of molecules due to the effective stirring of geometric profile. Due to an increase in friction time, the weld zone attains reverse plastic deformation based on Orowan strengthening [24]. Certain layers of unbounded copper particles were located on the stainless steel zone. The defects include the formation of kissing bonds, zigzag lines, and interlaminar cracks observed on the stainless steel phases. Macro voids and tunnel defects were observed in the intermetallic zones.

4. CONCLUSIONS

This work concludes on the joining of dissimilar alloys using the novel rotary welding mechanism through the variation in geometric patterns of the rubbing profiles, the following conclusion could be drawn.

1. The ultimate tensile strength values are maximumfor the helical profile compared to the other three, the values are optimal at a speed of 1100 rpm, and they gradually reduce to low values at 1500 rpm. The Ultimate tensile strength for the helical rubbing profile is 210 MPa, at 1100 rpm, at the same speed it is 205 MPa for a plus profile.
2. For a flat rubbing profile at the same speed the micro-Vickers hardness is found to be 97 HV, on the lower side at a speed of 1500 rpm the micro-Vickers hardness for a helical profile is 119 HV, for plus profile at the

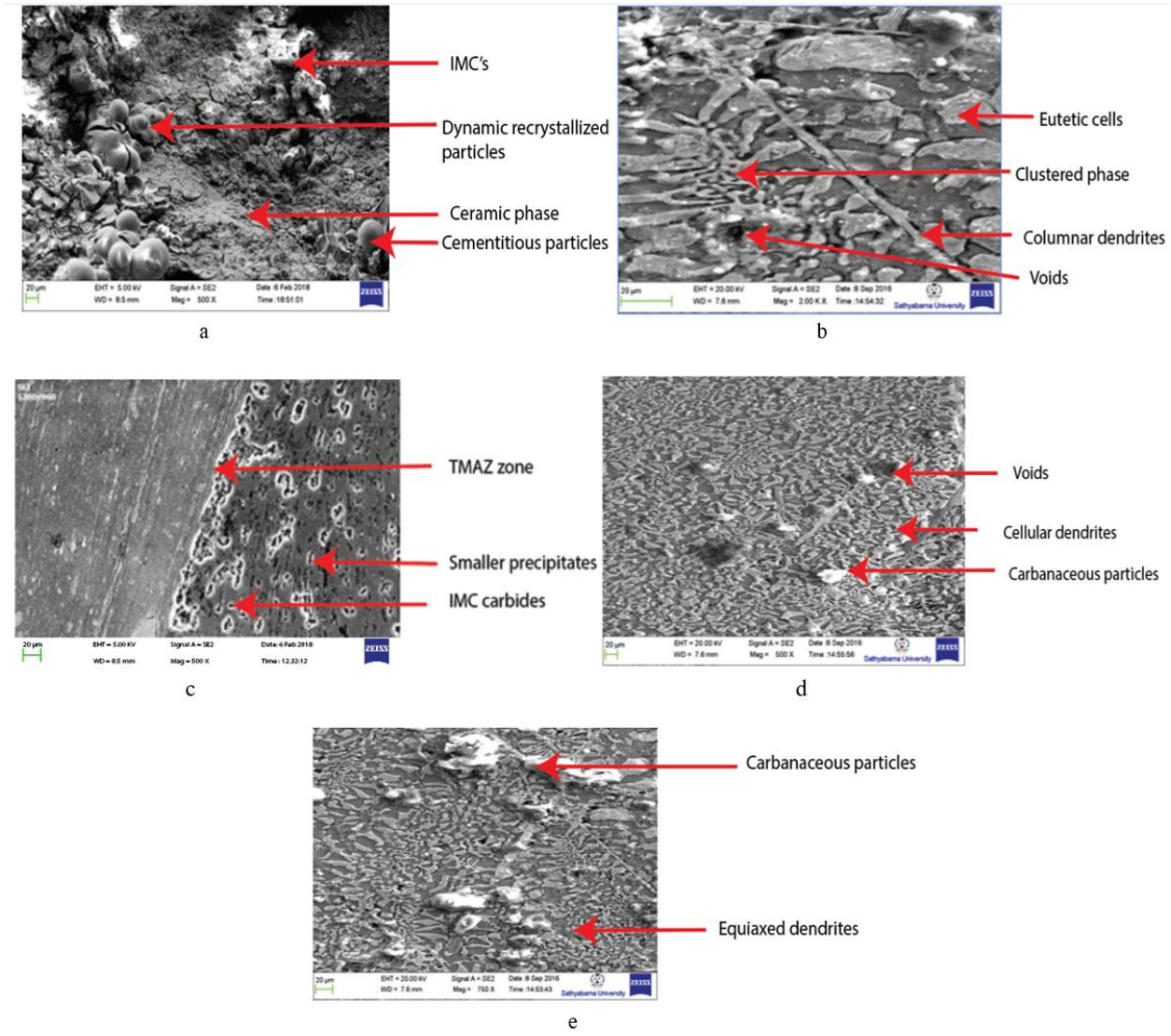

Fig. 8. Microstructural SEM images of helical fluke rubbing profile on various process parameters: a – rotational speed; b – friction time; c – friction pressure; d – upset pressure; e – upset time

same speed the micro-Vickers hardness is 101 HV, while forcylindrical profile the micro-Vickers hardness at that speedis 95 HV and for flat profile the micro Vickers hardness is 85 HV at the same speed.

3. It has been noted that the formation of intergranular layers has occurred at the thermo-mechanical affected zone. Some dendrites scars of SS316L have been observed in the TMAZ zone.
4. The cleavage factes were observed on the river flow pattern of the weldment. The extinction of copper and the formation of ultra-fine grains where occurred based on the boundary layer. Cracking of molecules over the nugget zones of SS and copper phase due to the effective stirring/alloying of geometric profile leads to the formation of carbonaceous IMCs with the MWCNT particles.
5. Further work could be carried out with the involvement of other efficient nano additives like MoS_2, graphene, alumina etc. at the weld interface to form the metal matrix composite joints that could improve the mechanical strength.

REFERENCES

1. **Flipo, B., Beamish, K., Humphreys, B., Wood, M.** Linear Friction Welding of Ti6Al4V for Aerostructure Applications *Proceedings of the 10th International Conference on Trends in Welding Research* 2016. https://doi.org/10.1155/2019/4728213
2. **Daya, W., Mohammad, H.V., Saeed, D., Ali Hussein, D.A., Andrés, A.C., Alfilh, R.H.C.** Wear Properties of Al/TiO_2 Composites Fabricated Via Combined Compo-casting and APB Process *Journal Science and Engineering of Composite Materials* 29 2022: pp. 535 – 545. https://doi.org/10.1515/secm-2022-0177
3. **Waluyo, A.S., Andrés, A.C., Kareem, A.K., Mohammad, H.V., Saeed, D.** Mechanical and Wear Evolution of Hybrid Al Composites Reinforced with Graphite and Blast Furnace Particles *Surface Review and Letters* 30 (3) 2023: pp. 2350011. https://doi.org/10.1142/S0218625X23500117
4. **Weining, W., Mohammad, H.V., Saeed, D.** Mechanical and Wear Properties of Al/TiC Composites Fabricated Via Combined Compo-Casting and APB Process *Feature Papers*

on Hybrid and Composite Crystalline Materials 12 (10) 2022: pp. 1440.
https://doi.org/10.3390/cryst12101440

5. **Mohammad, H.V., Omid, H.Z.** Significant Enhancement of Bond Strength in the Roll Bonding Process Using Pb Particles *International Journal of Materials Research* 109 2018: pp. 42 – 49.
https://doi.org/10.3139/146.111575
6. **Aisha, K.M., Abdulfadhil Gatea, M., Taif, A., Kareem, A.K., Heydari Vini, M., Daneshmand, S.** Theoretical and Experimental Study of the Roll Bonding Behavior of Bilayers Al Laminates *Surface Review and Letters* 30 (03) 2023: pp. 2350017.
https://doi.org/10.1142/S0218625X23500178
7. **Mohammad, H.V., Saeed, D.** Effect of Al_2O_3 Particles on the Mechanical and Wear Properties of Al Base Composites *Proceedings of the Institution of Mechanical Engineers, Part C: Journal of Mechanical Engineering Science* 2022: pp. 1 – 6.
https://doi.org/10.3390/cryst12101440
8. **Saade, A.J., Heydari Vini, M., Daneshmand, S.** Bonding Properties of Al/Al_2O_3 Bulk Composites Produced Via Combined Stir Casting and Accumulative Press Bonding *Surface Review and Letters* 29 (4) 2022: pp. 2250052.
https://doi.org/10.1142/S0218625X22500524
9. **Uday, M.B., Ahmad Fauzi, M.N., Zuhailawati, H., Ismail, A.B.** Advances in Friction Welding Process: A Review *Science and Technology of Welding and Joining* 15 (7) 2010: pp. 534 – 558.
https://doi.org/10.1179/136217110X12785889550064
10. **Chamanfar, A., Jahazi, M., Cormier, J.** A Review on Inertia and Linear Friction Welding of Ni- Based Superalloys *Metallurgical and Materials Transactions A* 46 (4) 2015: pp. 1639 – 1669.
https://doi.org/10.1007/S11661-015-2752-4
11. **Bhamji, I., Preuss, M., Threadgill, P.L., Moat, R.J., Addison, A.C., Peel, M.J.** Linear Friction Welding of AISI 316L Stainless Steel *Material Science and Engineering: A* 528 (2) 2010: pp. 680 – 690.
https://doi.org/10.1016/J.Msea.2010.09.043
12. **McAndrew, A.R., Colegrove, P.A., Addison, A.C., Flipo, B.C.D., Russell, M.J., Lee, L.A.** Modelling of the Workpiece Geometry Effects on Ti-6Al-4V Linear Friction Welds *Materials & Design* 87 2015: pp. 1087 – 109.
https://doi.org/10.1016/J.Matdes.2015.09.080
13. **Shanjeevi, C., Satish Kumar, S., Sathiya, P.** Multi-Objective Optimization of Friction Welding Parameters in AISI 304L Austenitic Stainless Steel and Copper Joints *Proceedings of the Institution of Mechanical Engineers, Part B: Journal of Engineering Manufacture* 230 (3) 2014: pp. 449 – 457.
https://doi.org/10.1177/0954405414555590
14. **Kumar, R., Balasubramanian, M.** Experimental Investigation of Ti–6Al–4V Titanium Alloy and 304L Stainless Steel Friction Welded with Copper Interlayer *Defence Technology* 11 (1) 2015: pp. 65 – 75.
https://doi.org/10.1016/j.dt.2014.10.001
15. **Lee, W.B., Jung, S.B.** Effect of Microstructural Variation on The Cu/CK45 Carbon Steel Friction Weld Joint *International Journal of Materials Research* 94 (12) 2003: pp. 1300 – 1306.
https://doi.org/10.1515/ijmr-2003-0235
16. **Li, W., Vairis, A., Preuss, M., Ma, T.** Linear and Rotary Friction Welding Review *International Materials Reviews* 61 (2) 2016: pp. 71 – 100.
https://doi.org/10.1080/09506608.2015.1109214
17. **Dalgaard, E.C.** Evolution of Microstructure, Micro-texture and Mechanical Properties in Linear Friction Welded Titanium Alloys *Canadian Journal of Metallurgy and Materials Science* 51 (2) 2012: pp. 269 – 276.
https://doi.org/10.1515/ijmr-2003-0235
18. **Avinash, M., Chaitanya, G.V.K., Giri, D.K., Upadhya, S., Muralidhara, B.K.** Microstructure and Mechanical Behaviuor of Rotary Friction Welded Titanium Alloys *International Journal of Materials and Metallurgical Engineering* 1 (11) 2007: pp. 641 – 643.
https://doi.org/10.5281/zenodo.1078985
19. **Palanivel, R., Laubscher, R.F., Dinaharan, I., Hattingh, D.G.** Microstructure and Mechanical Characterization of Continuous Drive Friction Welded Grade 2 Seamless Titanium Tubes at Different Rotational Speeds *International Journal of Pressure Vessels and Piping* 154 2017: pp. 17 – 28.
https://doi.org/10.1016/j.ijpvp.2017.06.005
20. **Midling, O.T., Grong, Ø.** A Process Model for Friction Welding of Al-Mg-Si Alloys and Al-SiC Metal Matrix Composites-I. HAZ Temperature and Strain Rate Distribution *Acta Metallurgica et Materialia* 42 (5) 1994: pp. 1595 – 1609.
https://doi.org/10.1016/0956-7151(94)90369-7
21. **Schroeder, F., Ward, R.M., Turner, R.P., Attallah, M.M., Gebelin, J.C., Reed, R.C.** Linear Friction Welding of Titanium Alloys for Aeroengine Applications: Modelling and Validation *Proceedings of 9th International Conference on Trends in Welding Research* 2012: pp. 886 – 892.
22. **Chen, G., Ren, C., Qin, X., Li, J.** Temperature Dependent Work Hardening in Ti-6Al-4V Alloy OverLarge Temperature and Strain Rate Ranges: Experiments and Constitutive Modeling *Materials & Design* 83 2015; pp. 598 – 610.
https://doi.org/10.1016/j.matdes.2015.06.048
23. **Johnson, G.R., Cook, W.H.** A Constitutive Model and Data for Metals Subjected to Large Strains, HighStrain Rates and High Temperatures *Proceedings of the 7th International Symposium on Ballistics* 1983: pp. 541 – 547.
24. **Ho Thi, Y., Truyen, T.L., Luu, P.M., Nguyen, H.L.A.** Study on Rotary Friction Welding of Titanium Alloy (Ti6Al4V) *Advances in Materials Science and Engineering* 2019: pp. 4728213.https://doi.org/10.1155/2019/4728213